First-principles study of boron speciation in calcite and aragonite

Etienne Balan, Fabio Pietrucci, Christel Gervais, Marc Blanchard, Jacques Schott, Jérome Gaillardet

HAL Id: hal-01371923

https://hal.sorbonne-universite.fr/hal-01371923

Submitted on 26 Sep 2016

First-principles study of boron speciation in calcite and aragonite

Revision 1

Etienne Balan[a,*], Fabio Pietrucci[a], Christel Gervais[b], Marc Blanchard[a],

Jacques Schott[c], Jérome Gaillardet[d]

[a]Sorbonne Universités - Institut de Minéralogie, de Physique des Matériaux et de Cosmochimie (IMPMC), UPMC Université Paris 06, UMR CNRS 7590, UMR IRD 206, MNHN, 4 place Jussieu, 75252 Paris cedex 05, France

[b]Sorbonne Universités - Laboratoire de Chimie de la Matière Condensée de Paris (LCMCP), UPMC Université Paris 06, UMR CNRS 7574, 4 place Jussieu, 75252 Paris cedex 05, France

[c]Géosciences Environnement Toulouse, Observatoire Midi-Pyrénées, CNRS-Université de Toulouse, 14, avenue Edouard Belin 31400 Toulouse, France

[d]Institut de Physique du Globe de Paris, Sorbonne Paris Cité, Université Paris Diderot, CNRS, F-75005 Paris, France, and Institut Universitaire de France.

[*]Corresponding author: Prof. Etienne Balan, Institut de Minéralogie, Physique des Matériaux et Cosmochimie, Case 115, 4 Place Jussieu, 75252 Paris Cedex 05.
tel: 00.33.1.44.27.74.52 fax: 00.33.1.44.27.37.85 E-mail: Etienne.Balan@impmc.upmc.fr

27   **Abstract**

28   Despite the importance of boron as a proxy of past ocean pH, the crystal-chemical

29   factors controlling its incorporation in the structure of calcium carbonates are still

30   poorly understood. This is partly linked to an imperfect knowledge of the coordination,

31   protonation state and local environment of boron species in these minerals. In the

32   present study, we use first-principles quantum mechanical tools to model selected

33   trigonal and tetragonal boron species in calcite and aragonite. The stable geometry of

34   the models is obtained from standard energy minimization schemes or using a more

35   advanced metadynamics exploration of their configurational space. The computation of

36   ^{11}B NMR chemical shifts and quadrupolar coupling parameters enables a

37   straightforward comparison of the models to existing experimental NMR data. The

38   results show that B in calcium carbonates does occur as structural species substituted

39   for CO_3^{2-} anions. The B speciation depends on the polymorph considered. In calcite,

40   structural boron is present as partially deprotonated trigonal $BO_2(OH)^{2-}$ species

41   coexisting with a fraction of substituted $B(OH)_4^-$ groups. In aragonite, the $B(OH)_4^-$

42   substitution for CO_3^{2-} anions is dominant. Different species, including entrapped $B(OH)_3$

43   molecules and substituted BO_3^{3-} groups also occur in biogenic samples. The diversity of

44   B speciation reflects a diversity of B incorporation mechanisms and sheds light on

45   previous studies confronting B isotopic composition determination with NMR

46   observations. The mechanisms of boron incorporation in calcium carbonates are

47   probably more complex than usually assumed in the literature using boron isotopes as a

48   proxy of paleo-atmospheric CO_2 reconstructions. Although not invalidating the empirical

49   paleo-pH proxy, these results call for a better understanding of the fundamental

50   mechanisms of boron incorporation in carbonates.

51

1. INTRODUCTION

The isotopic composition of boron in biogenic calcite and aragonite has been proposed and successfully used as a proxy of the past ocean acidity, which in turn reflects past levels of atmospheric CO_2 concentrations (Vengosh et al. 1991; Hemming and Hanson 1992). A large number of studies have applied this idea to various biogenic carbonates, proposed paleo-CO_2 secular evolutions for the Earth's atmosphere and established the sensitivity of global climate to atmospheric CO_2 in the past (e.g., Spivack et al. 1993; Gaillardet and Allègre 1995; Sanyal et al. 1995; Palmer et al. 1998; Pearson and Palmer 1999; Lemarchand et al. 2002; Pagani et al. 2005; Pearson et al. 2009; Martinez-Boti et al. 2015). The use of boron isotopes as a paleo-pH meter is based on the large difference in $^{11}B/^{10}B$ ratio (27.2 ‰ in delta notation of isotopic abundances; Klochko et al. 2006) occurring between the major dissolved forms of boron, the trigonal boric acid ($B(OH)_3$, preferentially enriched in ^{11}B), and the tetragonal borate ion ($B(OH)_4^-$, preferentially enriched in ^{10}B), under thermodynamic equilibrium conditions (Zeebe 2005; Liu and Tossell 2005; Klochko et al. 2006; Rustad et al. 2010; Nir et al. 2015). As the relative proportion of these aqueous species is strongly pH-dependent in the range of expected seawater pH, mass balance considerations require that their isotopic composition is also pH-dependent. Assuming that among the two major B species present in seawater only the borate ion ($B(OH)_4^-$) is incorporated in the mineral structure during crystal growth and that no boron isotope fractionation occurs during uptake, the B isotopic composition in marine carbonate samples provides a straightforward record of the secular variations of seawater pH.

The assumption of sole $B(OH)_4^-$ incorporation is challenged by spectroscopic studies reporting various proportions of both trigonal and tetragonal B species

coexisting in calcite and aragonite samples. Both boron partitioning and speciation are polymorph dependent, aragonite incorporating tetragonal boron more easily than calcite (e.g. Sen et al. 1994; Branson et al. 2015; Mavromatis et al. 2015). Direct determination of the boron coordination state can be achieved using [11]B solid-state nuclear magnetic resonance (NMR) (Sen et al. 1994; Klochko et al. 2006; Rollion-Bard et al. 2011; Mavromatis et al. 2015), electron energy loss spectroscopy (EELS) (Rollion-Bard et al. 2001) and scanning transmission X-ray microscopy (STXM) (Branson et al. 2015). The observation of an often dominant contribution of trigonal B in calcite, and its occurrence in aragonite, has been interpreted as reflecting a coordination change of borate ions at the surface of growing crystals (Hemming et al. 1998; Klochko et al. 2009; Branson et al. 2015). This interpretation is consistent with in-situ Atomic Force Microscopy (AFM) observations of the morphology and dynamic of the surface of calcite crystals growing from B-bearing solutions (Ruiz-Agudo et al. 2012). According to this mechanism, the boron isotopic composition in the mineral phase still reflects that of the borate ions in the solution. This explains the success of the boron-isotope proxy for paleo-pH reconstitutions from mineral remains of extinct species. However, several studies have suggested that a fraction of incorporated B could correspond to boric acid molecules, directly scavenged from the solution (Xiao et al. 2008, Rollion-Bard et al. 2011, Noireaux et al. 2015). Consistently, higher than expected [11]B/[10]B ratio have been determined on inorganically precipitated and biogenic calcium carbonate samples. Isotopic effects in biogenic carbonates have also been shown to depend upon the calcifying species. Although local variations of pH at the calcification site can surely contribute to the isotopic variability observed in biologically produced calcium carbonates, inorganic precipitation experiments under well-constrained pH conditions

101 cannot be reconciled with models based on the exclusive incorporation of borate ions,

102 showing that the basis hypotheses of the paleo-pH theory are questionable.

103   Despite the importance of the boron-isotope pH proxy, the crystal-chemical

104 factors controlling boron incorporation in carbonates are still elusive. Several factors

105 impede a detailed understanding of its incorporation mechanisms. Differences between

106 the geometry of the stiff molecular tetragonal B anions and that of the trigonal

107 substitution sites can lead to substantial modifications of the medium-range structure

108 around the B species. Various electrostatic charge compensation mechanisms (e.g.

109 involving different protonation states, presence of vacancies, or incorporation of other

110 trace elements) can also affect the B environment, which significantly increases the

111 system complexity. These effects are difficult to determine from experiment because

112 spectroscopic methods usually provide information restricted to the well-defined first

113 coordination shell of boron. Complementary to experimental observations, theoretical

114 approaches can bring important constraints to discuss molecular-scale aspects of B

115 incorporation in calcium carbonates. Tossell (2005, 2006) has investigated the NMR

116 spectroscopic and the thermodynamic properties of boron species using molecular

117 modeling techniques. Although these studies mostly focused on B species in aqueous

118 solutions and did not treat explicitly the role of the crystalline matrix, they provided

119 quantitative relations between the geometry and protonation state of the boron

120 complexes and their distinctive NMR parameters. In the light of the experimental data of

121 Sen et al. (1994), Tossell (2005) suggested that the incorporation of trigonal B should

122 occur via a distorted, partially deprotonated group instead of more symmetric fully

123 protonated or deprotonated groups. Tossell (2006) and Klochko et al. (2009) also

124 suggested that chemically more complex species such as $B(OH)_2CO_3^-$ could account for

125 the experimental observations of Sen et al. (1994).

126   In this article, we use first-principles quantum mechanical calculations to

127   determine the most favorable coordination states and geometry of boron species in

128   calcite and aragonite and discuss related incorporation mechanisms. We theoretically

129   determine the stable configuration of atomic-scale models of boron in calcium

130   carbonates, using an approach similar to that previously developed to study sulfate

131   incorporation in carbonates (Balan et al. 2014). The computation of the related NMR

132   parameters (Pickard and Mauri 2001; Charpentier 2011; Bonhomme et al. 2012) then

133   enables a straightforward comparison of the theoretical models to existing NMR

134   experimental data. The results attest to the diversity of B speciation in synthetic and

135   biogenic calcium carbonates; among which the substitution of partially protonated

136   trigonal $BO_2(OH)^{2-}$ and fully protonated tetragonal $B(OH)_4^{-}$ groups for CO_3^{2-} anions are

137   dominant.

138

139

140   **2. METHODS**

141

142   **2.1 Structural optimization of models of boron-bearing calcium carbonates**

143

144   First-principles quantum mechanical calculations provide the electronic density

145   and total energy of a system made of nuclei and electrons by solving the corresponding

146   Schrödinger equation. Many properties of a system (e.g. equilibrium structure, elastic

147   constants, vibrational modes, ...) are in fact determined by the total energy and its

148   variations. These methods are considered as highly predictive because their ingredients

149   are not fitted on experimental data. All of them are however characterized by a trade-off

150   between computation time and accuracy. In the past twenty years, methods based on

the density functional theory (DFT) have reached a level of accuracy high enough to reproduce with an excellent agreement the static and dynamic properties of geochemically relevant systems (see, e.g., Cygan and Kubicki 2001). The present calculations were performed within the DFT framework, using periodic boundary conditions and the generalized gradient approximation (GGA) to the exchange-correlation functional as proposed by Perdew, Burke and Ernzerhof (PBE; Perdew et al. 1996). The ionic cores were described by ultra-soft pseudopotentials from the GBRV library (Garrity et al. 2014); which means that only the electrons contributing to chemical bonding are explicitly treated, while those occupying the core states are considered to be unaffected by variations in the atom environment. The electronic wave-functions and charge density were expanded using a finite basis sets of plane-waves with 40 and 200 Ry cutoffs, respectively, corresponding to a convergence of the total energy better than 1 mRy/atom.

Periodic models of boron-bearing calcium carbonates were built for the two common $CaCO_3$ polymorphs: calcite ($R\bar{3}c$, 10 atoms per rhombohedral primitive cell) and aragonite (*Pmcm*, 20 atoms per primitive cell). In order to minimize as much as possible spurious interactions between the periodic images of the boron defects, the unit-cell of the models was built from the 2x2x2 super-cells of calcite (rhombohedral cell, 80 atoms) and aragonite (160 atoms) previously used in Balan et al. (2014). The equilibrium geometry of these models was obtained by displacing the atoms up to a minimum energy state, characterized by the fact that the forces experienced by the atoms vanish. These structure relaxations were done using the PWscf code of the Quantum ESPRESSO package (Giannozzi et al. 2009; http://www.quantum-espresso.org) and forces on atoms were minimized to less than 10^{-4} Ry/a.u. The

175   Brillouin zone sampling was restricted to a single *k*-point; which is appropriate to treat

176   such systems with large unit-cell.

177   A reference theoretical sassolite (boric acid; $B(OH)_3$) structure was obtained

178   using a 2x2x2 *k*-points grid. The relaxed cell volume (V = 285.28 $Å^3$) and bond lengths

179   (d(B-O) = 1.378 Å; d(O-H) = 1.01 Å) slightly overestimate their experimental

180   counterparts (V = 273.62 $Å^3$; d(B-O) = 1.36 Å; d(O-H) = 0.9 Å; Zachariasen 1954), which

181   is consistent with a previous DFT-GGA modeling study (Ferlat et al. 2006). A theoretical

182   structure of takedaite ($Ca_3B_2O_6$) was also obtained with a 2x2x2 *k*-points grid, leading to

183   relaxed cell volume (V = 785.23 $Å^3$) and bond lengths (d(B-O) = 1.391 Å) slightly larger

184   than experimental values (V = 765.61 $Å^3$, d(B-O) = 1.384 Å; Vegas et al. 1975).

185

186   **2.2 First-principles metadynamics**

187

188   First-principles metadynamics (Laio and Parrinello 2002) runs were used to

189   determine the most stable configuration of $B(OH)_4^-$ in its crystal host from an

190   exploration of the free-energy landscape drawn by variations in the H-bonding pattern.

191   This approach provides an efficient method to explore a free-energy landscape

192   potentially displaying several relative minima separated by barriers higher than the

193   relevant thermal energy. Usual molecular dynamics would require prohibitively high

194   temperature and/or long simulation to achieve an adequate sampling of the

195   corresponding phase space. In contrast, the metadynamics builds an history dependent

196   bias potential which drives the system away from the previously explored

197   configurations, thus accelerating the exploration of the phase space and providing an

198   elegant way to pass the energy barriers. In practice, the bias potential is built in a space

199   of reduced dimensionality depending on the properties under study and referred to as

200   collective variables space. For example, a chemical reaction can be described by

201   selecting a specific inter-atomic distance reflecting the breaking or the formation of a

202   chemical bond. In the present study, exploring the different possible configurations of a

203   given tetragonal boron group with respect to the calcite/aragonite crystal host equates

204   to exploring different topologies in the network of chemical interactions formed by

205   covalent and hydrogen bonds in a boron-centered region.

206   Born-Oppenheimer metadynamics runs were performed in the NVT ensemble

207   (i.e. the number of atoms, volume and average temperature were constant during the

208   runs) using the same DFT framework and parameters as those used for the structural

209   relaxations. The hydrogen mass was increased to two atomic mass units and the runs

210   were carried out with a timestep of 0.4 x 10^{-15} s. Temperature was controlled to 300 K

211   employing a stochastic velocity rescaling thermostat (Bussi et al. 2007). Both in

212   aragonite and calcite, we employed SPRINT collective variables (Pietrucci and Andreoni

213   2011), as implemented in Plumed (Bonomi et al., 2009), including a total of 26 atoms,

214   namely the 4 hydrogens belonging to $B(OH)_4^-$ and 22 oxygens belonging to carbonates

215   and lying within 4 Å of the oxygens belonging to $B(OH)_4^-$. The 26 collective variables

216   were biased simultaneously adding every 100 molecular dynamics steps Gaussian hills

217   of height 5.2 kJ/mol and width 0.9 or 1.1 (for aragonite or calcite, respectively).

218   To facilitate the identification of the different metastable configurations explored

219   along the metadynamics trajectory, we performed a structural cluster analysis in the

220   space of SPRINT collective variables, employing the k-medoids algorithm as

221   implemented in the software piv-clustering (Gallet and Pietrucci 2013).

222

223   **2.3 First-principles calculation of NMR parameters**

224

225   The I = 3/2 nuclear spin of ^{11}B implies that its NMR properties involve both the

226   Zeeman effect and the interaction of the nuclear quadrupolar moment with the electric

227   field gradient at the nucleus. Accordingly, three parameters can be extracted from ^{11}B

228   NMR spectra, namely the chemical shift δ_{iso}, the quadrupolar coupling constant C_Q and

229   the asymmetry parameter η.

230   The NMR chemical shift describes the difference between the applied external

231   magnetic field and the magnetic field at the nucleus positions. It can be obtained from

232   the structural models by calculating the shielding of the nuclei relative to the electronic

233   current induced by the external magnetic field. This current was calculated by using the

234   GIPAW approach, which allows reconstructing the all-electron magnetic response from

235   the pseudo-wave-functions (Pickard and Mauri 2001; Charpentier 2011; Bonhomme et

236   al. 2012). The calculations were performed using the PWscf and GIPAW codes of the

237   Quantum ESPRESSO package (Giannozzi et al. 2009). Norm-conserving pseudo-

238   potentials were used and the wave functions kinetic energy cutoff was increased to 80

239   Ry. The integral over the Brillouin zone was done using a Monkhorst-Pack 1×1×1 k-

240   point grid for the different models and 2×2×2 for sassolite (B(OH)$_3$) used as a reference.

241   The isotropic chemical shift δ_{iso} is defined as $\delta_{iso} = -(\sigma - \sigma^{ref})$, where σ is the isotropic

242   shielding (one-third of the trace of the NMR shielding tensor) and σ^{ref} is the isotropic

243   shielding of the same nucleus in a reference system. In our calculations, absolute

244   shielding tensors are obtained. To fix the scales, σ^{ref} was chosen by comparing

245   experimental (19.2 ppm, Soraru et al. 1999) and calculated δ_{iso} values in B(OH)$_3$.

246   The C_Q and η parameters are related to the eigenvalues of the electric field

247   gradient tensor and reflect the symmetry of the B environment. The $C_Q = 2.49$ MHz and

248    $\eta = 0.0$ parameters computed for sassolite (B(OH)$_3$) are consistent with experimental

10

249 values (2.47 MHz and 0.0; Klochko et al. 2009). It should be noted that for the $C_Q(^{11}B)$

250 calculation, a quadrupole moment of 35 mb was used: this value is smaller than the

251 theoretical value of 40 mb (Pyykkö, 2008) as recommended by Soleilhavoup et al.

252 (2010) in borosilicate glasses. Estimated precision is ±0.5 ppm, ±0.1 MHz and ±0.1 for

253 δ_{iso}, C_Q and η, respectively.

254

255 **3. RESULTS**

256

257 **3.1 Trigonal boron incorporation at the carbonate site**

258

259   We first consider the incorporation of trigonal boron species. The simplest model

260 is obtained by substituting a B^{3+} for a C^{4+} (Table 1). The charge balance is obtained by

261 spreading homogeneously an electrostatic counter-charge over the unit-cell. The crystal

262 site symmetry is preserved. The three equivalent B-O bonds in calcite have a length of

263 1.388 Å. The BO_3^{3-} group in aragonite displays a mirror symmetry with a shorter B-O

264 distance of 1.380 Å on the mirror plane and two symmetric B-O distances of 1.383 Å.

265 The high symmetry of BO_3^{3-} groups in the homogeneously compensated models leads to

266 very small η parameters. Compared to calcite, the aragonite ^{11}B chemical shift is higher

267 and similar to that of the calcium orthoborate, takedaite.

268   A more realistic charge compensation mechanism consists in adding one H atom

269 to the previous system, forming a $BO_2(OH)^{2-}$ group (Fig. 1). For the 3-fold calcite site, the

270 three oxygen atoms are symmetrically equivalent and only one protonation scheme was

271 considered. Two different protonation schemes are considered for aragonite, affecting

272 the oxygen on the mirror plane of the BO_3 triangle (scheme A) or one of the other two

273 symmetric oxygen atoms (scheme B). Scheme A is more stable than B by 16.8 kJ/mol

11

274   and should be thermodynamically dominant at room temperature. The $BO_2(OH)^{2-}$

275   species in calcite and aragonite display similar structural characteristics. The OH group

276   points out of the BO_3 triangle sharing a H-bond of moderate strength with an oxygen

277   belonging to an adjacent carbonate group. A significant distortion of the trigonal

278   geometry is observed with the B-O(H) distance increasing by ~ 0.1 Å; whereas the two

279   other B-O distances decrease by 0.03 to 0.04 Å. Compared to the models with an

280   homogeneous charge compensation, the ^{11}B δ_{iso} decreases by 1.5 and by 3 to 4 ppm in

281   calcite and aragonite, respectively; whereas the quadrupolar coupling parameter C_Q is

282   weakly affected. The asymmetry parameter η increases to 0.8 indicating a strong

283   departure from the revolution symmetry, consistent with the in-plane distortion of the

284   BO_3 triangle.

285

286   **3.2 Tetragonal boron incorporation at the carbonate site**

287

288   Following an approach similar to that applied to the trigonal B species, $B(OH)_4^-$

289   for CO_3^{2-} substitution was modeled by using a homogeneous electrostatic background to

290   compensate the charge imbalance. Previous calculations on sulfate incorporation in

291   carbonate (Balan et al. 2014) provided a suitable starting guess for the structural

292   optimization. However, the large number of potential H-bond acceptors around the

293   impurity increases the probability to drive the system to a metastable configuration.

294   This difficulty was circumvented by performing first-principles metadynamics (FPM)

295   runs (Laio and Parrinello 2002; Pietrucci and Andreoni 2011) to explore the free energy

296   landscape of the borate group conformation and to isolate the most favorable one.

297   The aragonite FPM run lasted $\sim 6 \times 10^{-12}$ s (Fig. 2, video file in electronic annex).

298   In an initial phase of $\sim 3 \times 10^{-12}$ s the instantaneous bias potential fluctuates between

299   zero and less than 10 kJ/mol, indicating that different configurations are being explored

300   (zero bias corresponds to an unexplored region of the configuration space). In a second

301   phase, the bias potential starts to grow more consistently to few tens of kJ/mol without

302   coming back to zero. This indicates that the available low-energy configurations have

303   been exhausted and that higher-energy configurations have been explored.

304   Concomitantly, the fluctuations of the SPRINT topological variables related to H and O

305   atoms (Fig. 2) attest to the changes of configuration of the $B(OH)_4^-$ species, by

306   reorienting the OH groups to engage in different patterns of hydrogen bonds with the

307   carbonates. The trajectory analysis leads to 8 maximally distinct instantaneous

308   configurations. After structural optimization, two classes of configurations differing by

309   the orientation of the O3-H bond (almost parallel to the b- axis or to the c-axis), could be

310   defined. In the following, only the most stable configuration will be considered since the

311   energy difference between the two (19 kJ/mol) is significantly larger than the typical

312   thermal energy at ambient temperature (2.5 kJ/mol). In this configuration (Fig. 1), the

313   O3-H bond is almost parallel to the c-axis and the borate group is slightly distorted with

314   an average B-O length of 1.481 Å (Table 1). As for sulfate (Balan et al. 2014), the borate

315   group is tilted with respect to the (a,b) plane and a significant displacement of the

316   neighboring carbonate groups is observed. The four H-bonds display quite regular

317   characteristics with O-H distances ranging from 0.989 to 1.008 Å and O(H)...O distances

318   from 2.62 to 2.65 Å. Few relative energy minima were however observed in each

319   configuration class due to moderate displacements of the surrounding carbonates,

320   leading to energy differences ranging between 5 and 13 kJ/mol. These configurations

321   can be envisioned as intermediate states in the transition from one H-bonding geometry

322   to the other. A longer FPM run (15×10^{-12} s, Fig. 3, video file in electronic annex) was

323   performed on calcite but only two different instantaneous configurations were

324   identified, leading to a single relaxed structure. As observed for other tetrahedral anions

325   in calcite (Reeder et al. 1994; Fernandez-Diaz et al. 2010; Balan et al. 2014), the $B(OH)_4^-$

326   anion is slightly tilted with the apical B-O bond forming an angle of 13° with respect to

327   the ternary axis of calcite. Although the structural environment is different, only slight

328   differences in the B-O and H-bond distances are observed between calcite and aragonite

329   (Table 1). The theoretical ^{11}B NMR parameters of $B(OH)_4^-$ in calcite and aragonite are

330   similar, with δ_{iso} close to 1 ppm and small quadrupolar coupling parameters (Table 1).

331   As for the trigonal B species, alternative models of tetragonal borate in calcium

332   carbonates were explored by assuming local charge compensation mechanisms.

333   Removing a proton from the $B(OH)_4^-$ group, modifies its charge to -2 (equivalent to that

334   of the CO_3^{2-} group). Starting from the tetrahedral geometries obtained from FPM runs,

335   four relaxed schemes (matching the four different H atoms of the borate group) are

336   obtained for each calcium carbonate polymorph. The deprotonation of the O3-H group

337   (Table 1) is favored in aragonite by more than 27 kJ/mol. In calcite, the most stable (by

338   more than 7 kJ/mol) configuration is obtained by deprotonation of the O2-H group

339   (Table 1). All the $BO(OH)_3^{2-}$ species display a significant distortion of the boron

340   coordination shell. Consistently, the C_Q values increase, ranging between 1.01 and 1.53

341   MHz.

342   A different mechanism ensuring the neutrality of $B(OH)_4^-$ for CO_3^{2-} substitution

343   corresponds to the coupled substitution of a monovalent cation for Ca^{2+}. Sodium is the

344   most relevant one both in terms of seawater abundance and ionic radii similarity. Two

345   configurations have been selected by assuming that the Na^+ for Ca^{2+} substitution affects

346   the site closest to the central boron atom (Fig. 1). In both configurations, the structure of

347   the $B(OH)_4^-$ group and the H-bonding pattern is weakly affected by the Na^+ for Ca^{2+}

348   substitution. The Na to B distances increase by ~0.05 Å compared to Ca to B distances.

14

349   Compared with the homogeneously compensated models, only weak variations of the

350   ^{11}B NMR parameters are observed (Table 1).

351

352   **4. DISCUSSION**

353

354   **4.1 Boron in calcium carbonates: Comparing theory and experiment**

355

356   4.1.1 Trigonal boron speciation

357

358   Although only few studies report experimentally determined NMR parameters of

359   boron in calcite and aragonite, they reveal a significant variability of the trigonal boron

360   environment (Table 2, Fig. 4). The chemical shift of trigonal boron ranges from 16 ppm

361   (calcite) to 22 ppm (heated aragonite) and strong differences are observed on the

362   rhombic η parameter. The trigonal boron species in the calcite samples investigated by

363   Sen et al. (1994) is rhombically distorted, with η values of 0.67 and 0.5 in the synthetic

364   and biogenic sample, respectively. In contrast, the nil η values reported by Klochko et al.

365   (2009) in biogenic calcite and aragonite samples correspond to a radially symmetric

366   environment of boron. A similarly low value of η is reported by Rollion-Bard et al.

367   (2011) for a biogenic aragonitic coral sample. As already highlighted by Klochko et al.

368   (2009), these variations in η values are highly significant because η is only defined

369   between 0 and 1.

370   The theoretical parameters determined for the $BO_2(OH)^{2-}$ species in calcite are

371   consistent with those reported by Sen et al. (1994) for synthetic calcite. The chemical

372   shift and quadrupolar coupling of $BO_2(OH)^{2-}$ in aragonite also match the experimental

373   values reported by Mavromatis et al. (2015) for synthetic aragonite. Unfortunately, the η

374   parameter was not reported for this sample, likely because of its low trigonal B content.

375   From the comparison of theoretical and experimental NMR parameters, singly

376   protonated $BO_2(OH)^{2-}$ groups appear as the dominant speciation of trigonal boron in the

377   synthetic calcium carbonates precipitated from solutions. This confirms the previous

378   suggestions that trigonal boron in carbonates should be distorted and partially

379   deprotonated (Hemming and Hanson 1992; Tossell 2005). This speciation is favored by

380   the electrostatic balance requirements. An overall preference for local electrostatic

381   charge compensation in minerals is attested by the observation of chemically complex

382   defects, associating different trace elements in the same crystal site. For example,

383   clumped-defects associating fluoride ions with carbonate groups have been observed in

384   apatite (Yi et al. 2013). Note however that, in absence of C_Q and η values, some

385   uncertainty affects the interpretation of the NMR parameters reported by Mavromatis et

386   al. (2015) for synthetic calcite samples. Their chemical shift is only slightly lower than

387   that of $BO_2(OH)^{2-}$ species and consistent with the value reported by Sen et al. (1994) for

388   a synthetic calcite sample (Fig. 4). Isotopic compositions (Noireaux et al. 2015) indicate

389   (under the assumption that no isotope fractionation occurs during incorporation) that

390   between 20% and 40% of boron in these samples results from the incorporation of

391   aqueous boric acid and that this proportion is linearly correlated with the pH-dependent

392   amount of boric acid in solution. The proportion of trigonal B detected by NMR is

393   however higher than that inferred from isotopic composition (Noireaux et al., 2015).

394   Thus, both borate anions and boric acid molecules could contribute to the incorporation

395   of $BO_2(OH)^{2-}$ species in the bulk of calcite particles. This implies a coordination change

396   of tetragonal borate as well as several deprotonation steps affecting the tetragonal and

397   trigonal boron species in the interfacial region of growing calcite crystals.

398   Concerning the biogenic calcium carbonates, the algal calcite investigated by Sen

399   et al. (1994) displays NMR parameters consistent with $BO_2(OH)^{2-}$ groups. In contrast,

400   the parameters reported by Klochko et al. (2009) for a foram calcite correspond to fully

401   deprotonated BO_3^{3-} groups substituted in the calcite structure (Fig. 4, Table 1). The

402   sensitivity of ^{11}B NMR to the trigonal boron protonation state is further confirmed by

403   the higher δ_{iso}, and weak η, indicative of a more symmetric boron environment in a

404   calcite sample produced by the high-temperature (500 °C) transformation of biogenic

405   aragonite. These parameters are close to those computed for BO_3^{3-} groups in aragonite

406   (Fig. 4) and in the calcium orthoborate takedaite (Table 1). They indicate that the

407   thermally driven aragonite to calcite transformation leads to a full deprotonation of

408   borate groups. They however suggest that the local environment of BO_3^{3-} groups in the

409   heated aragonite differs from that in crystalline calcite.

410   The ^{11}B NMR parameters of trigonal boron in coral aragonitic samples combine

411   comparatively low δ_{iso} value and weak η (Klochko et al. 2009; Rollion-Bard et al. 2011).

412   The weak η is indicative of a regular coordination shell, but the δ_{iso} values are too low to

413   correspond to fully deprotonated BO_3^{3-} groups (Fig. 4; Table 1). Accordingly, these

414   parameters are interpreted as related to fully protonated $B(OH)_3$ molecules. The

415   incorporation of boric acid molecules in crystallographic sites is unrealistic because of

416   the corresponding strong electrostatic charge imbalance. It is more likely that $B(OH)_3$

417   molecules are directly scavenged from the solution and encapsulated by the solid phase.

418   Such step can involve their incorporation in the amorphous and hydrous calcium

419   carbonate phases, observed under high supersaturation and elevated growth rate

420   conditions and identified as intermediate phases in the growth of biogenic calcium

421   carbonates (e.g. Gower 2008; Purgstaller et al., 2016). The $B(OH)_3$ molecules could also

422   occur in interfacial or porous regions separating ordered $CaCO_3$ nanodomains, such as

423   those observed in calcitic red coral (Vielzeuf et al. 2008). The preserved coordination

424   state and isotopic composition can lead to higher than expected $\delta^{11}B$, depending on the

425   proportion of $B(OH)_3$ molecules relative to the total B content. This interpretation is

426   consistent with the concomitant observation of elevated $\delta^{11}B$ and higher trigonal boron

427   concentration at the center of calcification of an aragonitic coral sample by Rollion-Bard

428   et al. (2011). Note however that trigonal B usually is a minority species in aragonitic

429   samples, which tempers the isotopic effect related to $B(OH)_3$ incorporation.

430

431   4.1.2 Tetragonal boron speciation

432

433   The experimental chemical shift of tetragonal B species displays a range of

434   variation between -2.4 and 3 ppm, considering both calcite and aragonite (Fig. 5). Except

435   two samples with δ_{iso} above 2 ppm and two signals with negative chemical shifts

436   ascribed to non-structural species in calcitic samples (Mavromatis et al. 2015), the NMR

437   parameters are consistent with those obtained for the $B(OH)_4^-$ models. The

438   systematically nil values of experimental quadrupolar coupling parameters (Table 2)

439   attest to a highly symmetric B environment. They rule out the partially deprotonated

440   tetragonal species, which are characterized by theoretical C_Q values larger than 1 MHz.

441   Accordingly, tetragonal B should mostly occur in the calcium carbonate samples as fully

442   protonated $B(OH)_4^-$ groups. A high protonation state of tetragonal B was suggested by

443   Klochko et al. (2009) from ^1H decoupling experiments.

444   The substitution of $B(OH)_4^-$ for CO_3^{2-} implies that more remote mechanisms

445   ensure the charge compensation, among which the Na^+ for Ca^{2+} substitution is the most

446   probable one. As a matter of fact, the Na-bearing models also display NMR parameters

447   consistent with the experimental observations. This coupled substitution could be

18

448   responsible, at least in part, for the dependence of B/Ca ratio on salinity reported for

449   biogenic calcium carbonates (Allen et al. 2011, 2012; Allen and Hönisch 2012; Henehan

450   et al. 2015). Inorganic co-precipitation experiments of Kitano et al. (1978) have also

451   shown a significant increase in B incorporation in calcite with increasing NaCl

452   concentration in the parent solution. For aragonite, the observed dependence was in the

453   opposite direction but with a comparatively weaker magnitude. We note however that

454   an aragonitic coral sample and an hydrothermal calcitic sample investigated by Klochko

455   et al. (2009) display higher δ_{iso} values of 2.54 and 2.87 ppm, respectively, and likely

456   correspond to $B(OH)_4^-$ groups in a different environment or involving a charge

457   compensation mechanism differing from that prevailing in the other samples. The

458   potential presence of contaminant phases cannot be fully excluded for these natural

459   samples. Beside Na^+ for Ca^{2+} substitution, different charge compensation mechanisms

460   could occur, as shown by the Na-free synthesis experiments of Hemming et al. (1995)

461   and Sen et al. (1994). For example, HCO_3^- groups associated with Ca vacancies could play

462   such compensation role. A potential role of phosphate anions substituted for carbonate

463   groups has also been suggested by Henehan et al. (2015). Variations in the borate group

464   environment are also attested by the broad signals with slightly negative chemical shifts

465   observed by Mavromatis et al. (2015), interpreted as corresponding to a fraction of

466   borate groups occurring in defective domains of the calcite samples.

467

468   **4.2 Boron speciation in calcium carbonates: Implications for the paleo-pH proxy**

469

470   The present results show that B in calcium carbonates does occur as substituted

471   species for CO_3^{2-} anions, thus confirming its structural nature. They further show that its

472   speciation depends on the polymorph considered. This is fully consistent with a number

473   of previous studies on boron incorporation in biogenic and abiotic carbonates (e.g.

474   Klochko et al. 2009; Mavromatis et al. 2015; Noireaux et al. 2015) and strongly challenge

475   the hypothesis on which the use of boron isotopes to reconstruct paleo ocean pH has

476   been used (i.e. sole incorporation of the aqueous borate ion). In calcite, structural boron

477   is present as partially deprotonated trigonal $BO_2(OH)^{2-}$ species, coexisting with

478   substituted $B(OH)_4^-$ groups in a proportion depending on the crystal growth parameters.

479   In aragonite, the $B(OH)_4^-$ substitution for CO_3^{2-} anions is dominant. The theoretical

480   modeling of NMR spectra also indicates that different B species, including entrapped

481    $B(OH)_3$ molecules and substituted BO_3^{3-} groups can occur in biogenic samples. The

482   diversity of B speciation indirectly confirms the importance of out-of-equilibrium

483   parameters and interfacial properties in determining the chemical form and abundance

484   of boron in calcium carbonate (e.g., Hemming et al. 1998; Hobbs and Reardon 1999;

485   Ruiz-Agudo et al. 2012; Gabitov et al. 2014; Branson et al. 2015; Noireaux et al. 2015;

486   Uchikawa et al. 2015; Kaczmarek et al. 2016). Although the $B(OH)_3$ molecules in

487   biogenic aragonitic samples might have been directly scavenged from the solution, the

488   other trigonal $BO_2(OH)^{2-}$ and BO_3^{3-} species most probably result from a coordination

489   change and deprotonation of boron species adsorbed at the mineral surface.

490   An important implication of the observed diversity of B speciation in calcium

491   carbonates is that the ratio of trigonal to tetragonal species determined by NMR

492   spectroscopy is not a sufficient parameter to infer its incorporation mechanism. This

493   ratio is not simply related to the trigonal to tetragonal proportion in the solution nor

494   solely results from a coordination decrease affecting the adsorbed borate ion during its

495   incorporation in the crystal structure. The environment and protonation state of

496   trigonal B however appears as more variable than that of the tetragonal species. In this

497   latter case, the variations are most likely related to more remote charge compensation

498 mechanisms and do not affect the first coordination shell of boron. In addition, the high

499 sodium concentration of seawater could favor the Na^+ for Ca^{2+} substitution in the charge

500 compensation of $B(OH)_4^-$ species. The prevalence of a specific charge compensation

501 mechanism would reduce the crystal-chemical complexity of the $B(OH)_4^-$ incorporation

502 mechanism. Interestingly, the affinity of aragonite is higher than that of calcite for both B

503 and Na. In the case of Na, this has been interpreted as reflecting its incorporation in

504 interstitial sites of calcite, instead of structural Ca site as in aragonite (Ishikawa and

505 Ichikuni 1984; Okumura et al. 1986). As a consequence, aragonitic samples in which

506 tetragonal B is dominant should faithfully reflect the pH of past oceans, as proposed by

507 Noireaux et al. (2015), provided that sampling strategies taking into account the growth

508 mechanism of biologic aragonite are developed (Rollion-Bard et al. 2011).

509   In the case of calcitic samples, the more diverse boron speciation could be

510 considered as a fingerprint of the growth mechanism and could serve as an indicator to

511 extrapolate the laboratory calibrations to the geologic samples. The recent spatially-

512 resolved study of Branson et al. (2015) indicates a dominantly trigonal (>85%)

513 coordination and a heterogeneous distribution of boron in foraminiferal calcite;

514 whereas NMR studies revealed a fraction of tetragonal B in biogenic calcite (~20%, Sen

515 et al. 1994; ~54%, Klochko et al. 2009). Thus, the occurrence of differently coordinated

516 species, with potentially distinct isotopic compositions, in spatially different domains of

517 the composite biogenic samples cannot be excluded. As diagenesis and alteration may

518 differently affect these domains, the boron isotopic composition of geological samples

519 would then depend on their preservation state (Wara et al. 2003). We note however that

520 the observations of Edgar et al. (2015) suggest that the boron isotopic composition of

521 fossil planktonic foraminiferal calcite is resistant to diagenetic transformations. This

522 calls for further experimental studies focusing on the effects of diagenesis on boron

523 speciation in carbonates.

524 Finally, we highlight that the approach developed in the present study, which

525 combines a metadynamics determination of stable configurations of polyatomic groups

526 with the first-principles calculation of related spectroscopic parameters, represents a

527 general tool to explore the speciation of molecular anions in host crystalline matrices,

528 readily applicable to a larger range of geochemical proxies in minerals.

529

537

538 **REFERENCES**

539 Allen K. A. and Hoenisch B. (2012) The planktic foraminiferal B/Ca proxy for seawater

540 carbonate chemistry: A critical evaluation, *Earth Planet. Sci. Lett.* **345–348**, 203–

541 21.

542 Allen K. A., Hoenisch B., Eggins S. M., Yu J., Spero H. J. and Elderfield H. (2011) Controls

543 on boron incorporation in cultured tests of the planktic foraminifer Orbulina

544 universa, *Earth Planet. Sci. Lett.* **309**, 291–30.

545   Allen K. A., Hoenisch B., Eggins S. M. and Rosenthal Y. (2012) Environmental controls on

546   B/Ca in calcite tests of the tropical planktic foraminifer species Globigerinoides

547   ruber and Globigerinoides sacculifer, *Earth Planet. Sci. Lett.* **351–352**, 270–280,

548   Balan E., Blanchard M., Pinilla C. and Lazzeri M. (2014) First-principles modeling of

549   sulfate incorporation and $^{34}S/^{32}S$ isotopic fractionation in different calcium

550   carbonates. *Chem. Geol.* **374-375**, 84-91.

551   Bonhomme C., Gervais C., Babonneau F., Coelho C., Pourpoint F., Azaïs T., Ashbrook S.E.,

552   Griffin J.M., Yates J.R., Mauri F. and Pickard C.I. (2012) First-Principles Calculation

553   of NMR Parameters using the gauge including projector augmented wave method:

554   A chemist's point of view. *Chemical reviews* **112**, 5733–5779.

555   Bonomi M., Branduardi D., Bussi G., Camilloni C., Provasi D., Raiteri P., Donadio D.,

556   Marinelli F., Pietrucci F., Broglia R.A. and Parrinello M. (2009) PLUMED: a portable

557   plugin for free-energy calculations with molecular dynamics. *Comp. Phys. Comm.*

558   **180**, 1961.

559   Branson O., Kaczmarek K., Refern S. A. T., Misra, S., Langer G., Tyliszczak T., Bijma J. and

560   Elderfield H. (2015) The coordination and distribution of B in foraminiferal calcite.

561   *Earth Planet. Sci. Lett.* **416**, 67-72.

562   Bussi G., Donadio D. and Parrinello M. (2007) Canonical sampling through velocity

563   rescaling. *J. Chem. Phys.* **126**, 014101.

564   Charpentier T. (2011) The PAW/GIPAW approach for computing NMR parameters: A

565   new dimension added to NMR study of solids. *Solid State NMR* **40**, 1-20.

566   Cygan, R.T. and Kubicki, J.D. (2001) Reviews in Minerology and Geochemistry: Molecular

567   Modeling Theory: Applications in the Geosciences. 531 p. The Mineralogical

568   Society of America, Washington, D.C.

569   Edgar K., Anagnostou E., Pearson P. and Foster G. (2015) Assessing the impact of

570   diagenesis on 11B, 13C, 18O, Sr/Ca and B/Ca values in fossil planktic foraminiferal

571   calcite. *Geochim. Cosmochim. Acta* **166**, 189- 209.

572   Ferlat G., Cormier L., Mauri F., Balan E., Charpentier T., Anglada E. and Calas G. (2006)

573   Ab initio calculations on borate systems. *Eur. J. Glass Sci. Techno. B* **4**, 441-444.

574   Fernández-Díaz L., Fernández-González A. and Prieto M. (2010) The role of sulfate

575   groups in controlling $CaCO_3$ polymorphism. *Geochim. Cosmochim. Acta* **74**, 6064-

576   6076.

577   Gabitov R. I., Rollion-Bard C., Tripati A. and Sadekov A. (2014) In situ study of boron

578   partitioning between calcite and fluid at different crystal growth rates. *Geochim.*

579   *Cosmochim. Acta* **137**, 81-92.

580   Gaillardet J. and Allègre C.J. (1995) Boron isotopic compositions of corals: Seawater or

581   diagenesis record? *Earth Planet. Sci. Lett.* **136**, 665-676.

582   Gallet G. A. and Pietrucci F. (2013) Structural cluster analysis of chemical reactions in

583   solution. *J. Chem. Phys.* **139**, 074101.

584   Garrity K. F., Bennett J. W., Rabe K. M. and Vanderbilt D. (2014) Pseudopotentials for

585   high-throuhput DFT calculations. *Comput. Mat. Sci.* **81**, 446-452.

586   Giannozzi P., Baroni S., Bonini N., Calandra M., Car R., Cavazzoni C., Ceresoli D., Chiarotti

587   G.L., Cococcioni M., Dabo I., Dal Corso A., de Gironcoli S., Fabris S., Fratesi G.,

588   Gebauer R., Gerstmann U., Gougoussis C., Kokalj A., Lazzeri M., Martin-Samos L.,

589   Marzari N., Mauri F., Mazzarello R., Paolini S., Pasquarello A., Paulatto L., Sbraccia

590   C., Scandolo S., Sclauzero G., Seitsonen A.P., Smogunov A., Umari P. and

591   Wentzcovitch R.M. (2009) Quantum ESPRESSO: a modular and open-source

592   software project for quantum simulations of materials. *J. Phys.: Cond. Matt.* **21**,

593   395502.

594 Gower L. B. (2008) Biomimetic model systems for investigating the amorphous
595   precursor pathway and its role in biomineralization. *Chem. Rev.* **108**, 4551–4627.

596 Henehan M. J., Foster G. L., Rae J. W. B., Prentice K. C., Erez J., Bostock H. C.,
597   Marshall B. J. and Wilson P. A. (2015) Evaluating the utility of B/Ca ratios in
598   planktic foraminifera as a proxy for the carbonate system: A case study of
599   Globigerinoides ruber. *Geochem. Geophys. Geosyst.* **16**, 1052–1069

600 Hemming N. G. and Hanson G. N. (1992) Boron isotopic composition and concentration
601   in modern marine carbonates. *Geochim. Cosmochim. Acta* **56**, 537-543.

602 Hemming N. G., Reeder R. J. and Hanson G. N. (1995) Mineral-fluid partitioning and
603   isotopic fractionation of boron in synthetic calcium carbonates. *Geochim.*
604   *Cosmochim. Acta* **59**, 371-379.

605 Hemming N. G., Reeder R. J. and Hart S. R. (1998) Growth-step-selective incorporation of
606   boron on the calcite surface. *Geochim. Cosmochim. Acta* **62**, 2915-2922.

607 Hobbs M. Y. and Reardon E. J. (1999) Effect of pH on boron coprecipitation by calcite:
608   Further evidence for nonequilibrium partitioning of trace elements. *Geochim.*
609   *Cosmochim. Acta* **63**, 1013-1021.

610 Ishikawa M. and Ichikuni M. (1984) Uptake of sodium and potassium by calcite. *Chem.*
611   *Geol.* **42**, 137-146

612 Kaczmarek K., Nehrke G., Misra S., Bijma J. and Elderfield H. (2016) Investigating the
613   effects of growth rate and temperature on the B/Ca ratio and δ^{11}B during inorganic
614   calcite formation. *Chem. Geol.* **421**, 81-92.

615 Kitano Y., Okumura M. and Idogaki (1978) Coprecipitation of borate-born with calcium
616   carbonate. *Geochemical Journal* **12**, 183-189.

617 Klochko K., Kaufman A. J., Yao W., Byrne R. H. and Tossell J. A. (2006) Experimental
618   measurement of boron isotope fractionation in seawater. *Earth Planet. Sci. Lett.*

619   **248**, 276-285.

620 Laio A. and Parrinello M. (2002) Escaping free-energy minima. *Proc. Nat. Acad. Sci.* **99**,

621   12562-12566.

622 Liu Y. and Tossell J. A. (2005) Ab initio molecular orbital calculations for boron isotope

623   fractionations on boric acids and borates. *Geochim. Cosmochim. Acta* **69**, 3995-

624   4006.

625 Lemarchand D., Gaillardet J., Lewin E. and Allègre C. J. (2002) Boron isotope systematics

626   in large rivers: implications for the marine boron budget and paleo-pH

627   reconstruction over the Cenozoic. *Nature* **408**, 951-954.

628 Martinez-Boti M. A., Marino G., Foster G. L., Ziveri P., Henehan M.J., Rae J. W. B., Mortyn P.

629   G. and Vance D. (2015) Boron isotope evidence for oceanic carbon dioxide leakage

630   during the last deglaciation. *Nature* **518**, 219-222.

631 Mavromatis V., Montouillout V., Noireaux J., Gaillardet J. and Schott J. (2015)

632   Characterization of boron incorporation and speciation in calcite and aragonite

633   from co-precipitation experiments under controlled pH, temperature and

634   precipitation rate *Geochim. Cosmochim. Acta* **150**, 299-313.

635 Nir O., Vengosh A., Harkness J. S., Dwyer G. S. and Lahav O. (2015) Direct measurement

636   of the boron isotope fractionation factor: Reducing the uncertainty in

637   reconstructing ocean paleo-pH. *Earth Planet. Sci. Lett.* **414**, 1-5.

638 Noireaux J., Mavromatis V., Gaillardet J., Schott J., Montouillout V., Louvat P., Rollion-Bard

639   C. and Neuville D. R. (2015) Crystallographic control on the boron isotope paleo-

640   pH proxy. *Earth Planet. Sci. Lett.* **430**, 398-407.

641 Okumura M. and Kitano Y. (1986) Coprecipitation of alkali metal ions with calcium

642   carbonate. *Geochim. Cosmochim. Acta* **50**, 49-58.

643   Pagani M., Lemarchand D., Spivack A and Gaillardet J. (2005) A critical evaluation of the

644   boron isotope-pH proxy: the accuracy of ancient ocean pH estimates. *Geochim.*

645   *Cosmochim. Acta* **69**, 953–961.

646   Palmer M. R., Pearson P. N. and Cobb S. J. (1998) Reconstructing past ocean pH-depth

647   profiles. *Science* **282**, 1468-1471.

648   Pearson P. N. and Palmer M. R. (1999) Middle eocene seawater pH and atmospheric

649   carbon dioxide concentrations. *Science* **284**, 1824-1826.

650   Pearson P. N., Foster G. L. and Wade B. S. (2009) Atmospheric carbon dioxide through

651   the Eocene-Oligocene climate transition. *Nature* **461**, 1110–1113.

652   Perdew J. P., Burke K. and Ernzerhof M. (1996) Generalized gradient approximation

653   made simple. *Phys. Rev. Lett.* **77**, 3865–3868.

654   Pickard C. and Mauri F. (2001) All-electron magnetic response with pseudopotentials:

655   NMR chemical shifts. *Phys. Rev. B* **63**, 245101.

656   Pietrucci F. and Andreoni W. (2011) Graph theory meets ab initio molecular dynamics:

657   atomic structures and transformations at the nanoscale. *Phys. Rev. Lett.* **107**,

658   085504.

659   Purgstaller B., Mavromatis V., Immenhauser A. and Dietzel M. (2016) Transformation of

660   Mg bearing amorphous calcium carbonate to Mg-calcite - In situ monitoring.

661   *Geochim. Cosmochim. Acta* **174**, 180-195.

662   Pyykkö P. (2008) Year-2008 nuclear quadrupole moments. *Mol. Phys.* **106**, 1065.

663   Reeder R. J., Lamble G. M., Lee J.-F. and Staudt W. J. (1994) Mechanism of SeO_4^{2-}

664   substitution in calcite: An XAFS study. *Geochim. Cosmochim. Acta* **58**, 5639-5646.

665   Rollion-Bard C., Blamart D., Trebosc J., Tricot G., Mussi A. and Cuif J.-P. (2011) Boron

666   isotops as a pH proxy: A new look at boron speciation in deep-sea corals using [11]B

667   MAS NMR and EELS. *Geochim. Cosmochim. Acta* **75**, 1003-1012.

668 Ruiz-Agudo E., Putnis C. V., Kowacz M., Ortega-Huertas M. and Putnis A. (2012) Boron
669   incorporation into calcite during growth: Implications for the use of boron in
670   carbonates as a pH proxy. *Earth Planet. Sci. Lett.* **345-348**, 9-17.

671 Rustad J. R., Bylaska E. J., Jackson V. E. and Dixon D. A. (2010) Calculation of boron-
672   isotope fractionation between $B(OH)_{3(aq)}$ and $B(OH)_{4\ (aq)}^{-}$. *Geochim. Cosmochim. Acta*
673   **74**, 2843-2850.

674 Sanyal A., Hemming N. G., Hanson G. N. and Broecker W. S. (1995) Evidence for a higher
675   *p*H in the glacial ocean from boron isotopes in foraminifera. *Nature* **373**, 234–236.

676 Sen S., Stebbins J. F., Hemming N. G. and Ghosh B. (1994) Coordination environments of
677   B impurities in calcite and aragonite polymorphs: A ^{11}B MAS NMR study. *Am.*
678   *Mineral.* **79**, 819-825.

679 Soleilhavoup A., Delaye J.-M., Angeli F., Caurant D. and Charpentier T. (2010)
680   Contribution of first-principles calculations to multinuclear NMR analysis of
681   borosilicate glasses. *Magn. Reson. Chem.* **48**, S159–S170.

682 Soraru G.D., Babonneau F., Gervais C. and Dallabona N. (2000) Hybrid $RSiO1{:}5/B_2O_3$ gels
683   from modified silicon alkoxides and boric acid. *J. Sol-Gel Sci. and Techno.* **18**, 11–19.

684 Spivack A. J., You C. and Smith H. J. (1993) Foraminiferal boron isotope ratios as a proxy
685   for surface ocean pH over the past 21 Myr. *Nature* **363**, 149-151.

686 Tossell J. A. (2005) Boric acid, "carbonic" acid, and N-containing oxyacids in aqueous
687   solution: Ab initio studies of structure, pKa, NMR shifts, and isotopic fractionations.
688   *Geochim. Cosmochim. Acta* **69**, 5647-5658.

689 Tossell J. A. (2006) Boric acid adsorption on humic acids: Ab initio calculation of
690   structures, stabilities, ^{11}B NMR and ^{11}B,^{10}B isotopic fractionations of surface
691   complexes. *Geochim. Cosmochim. Acta* **70**, 5089-5103.

692   Uchikawa J., Penman D. E., Zachos J. C. and Zeebe R. E. (2015) Experimental evidence of

693   kinetic effects on B/Ca in synthetic calcite: Implications for potential $B(OH)_4^-$ and

694        $B(OH)_3$ incorporation. *Geochim. Cosmochim. Acta* **150**, 171-191.

695   Vegas A., Cano F. H. and Garcia-Blanco S. (1975) The crystal structure of calcium

696   orthoborate: a redetermination. *Acta Crystallogr B* **31**, 1416-1419.

697   Vengosh A., Kolodny Y., Starinsky A., Chivas A. R. and McCulloch M. T. (1991) Copre-

698   cipitation and isotopic fractionation of boron in modern biogenic carbonates.

699   *Geochim. Cosmochim. Acta* **55**, 2901–2910.

700   Vielzeuf D., Garrabou J., Baronnet A., Grauby O. and Marschal C. (2008) Nano to

701   macroscale biomineral architecture of red coral (Corallium rubrum). *Amer.*

702   *Mineral.* **93**, 1799–1815.

703   Wara M. W., Delaney M. L., Bullen T. D. and Ravelo A. C. (2003) Possible roles of pH,

704   temperature, and partial dissolution in determining boron concentration and

705   isotopic composition in planktonic foraminifera. *Paleoceanography* **18(4)**, 1100,

706   doi:10.1029/2002PA000797

707   Xiao Y. K., Li H. L., Liu W. G., Wang X. F. and Jiang S. Y. (2008) Boron isotopic fractionation

708   in laboratory inorganic carbonate precipitation: Evidence for the incorporation of

709        $B(OH)_3$ into carbonate. *Sci. China Ser. D* **51**, 1776–1785.

710   Yi H., Balan E., Gervais C., Segalen L., Fayon F., Roche D., Person A., Morin G., Guillaumet

711   M., Blanchard M., Lazzeri M. and Babonneau F. (2013) A carbonate-fluoride defect

712   model for carbonate-rich fluorapatite. *Amer. Mineral.* **98**, 1066-1069.

713   Zachariasen W. H. (1954) The precise structure of orthoboric acid. *Acta Crystallogr.* **7**,

714   305-310.

715   Zeebe R. E. (2005) Stable boron isotope fractionation between dissolved $B(OH)_3$ and $B(OH)_4^-$

716   *Geochim. Cosmochim. Acta* **69**, 2753–2766.

717

718   Table 1: Structural and ^{11}B NMR parameters of boron-bearing calcium carbonate models

B coordinence	mineral	model	B-O bond length (Å)	O-H bond length (Å)	δ_{iso} (ppm)	C_Q (MHz)	η
trigonal	calcite	BO_3^{3-}	1.388 (x3)	-	19.10	2.73	0.00
		$BO_2(OH)^{2-}$	1.345 1.350 O(H) 1.491	- - 0.995	17.51	2.59	0.84
	aragonite	BO_3^{3-}	1.380 1.383 (x2)	-	22.04	2.74	0.04
		$BO_2(OH)^{2-}$ (A)	1.343 1.350 O(H) 1.472	- - 0.988	19.11	2.59	0.81
		$BO_2(OH)^{2-}$ (B)	1.347 1.349 O(H) 1.472	- - 0.991	18.14	2.57	0.82
	takedaite	BO_3^{3-}	1.391	-	22.11	2.74	0.00
tetragonal	calcite	$B(OH)_4^-$	O1 1.438 O3 1.477 O4 1.489 O2 1.510	1.005 1.002 0.997 0.996	1.05	0.43	0.57
		$BO(OH)_3^{2-}$	O2 1.402 O1 1.494 O3 1.524 O4 1.532	- 0.996 0.996 0.994	1.29	1.09	0.34
		$B(OH)_4^-,Na^+$	O1 1.434 O3 1.470 O4 1.499 O2 1.522	1.006 0.993 0.997 0.992	1.15	0.56	0.67
	aragonite	$B(OH)_4^-$	O2 1.455 O1 1.476 O4 1.497 O3 1.497	0.992 1.008 0.989 1.003	0.81	0.22	0.50
		$BO(OH)_3^{2-}$	O3 1.402 O2 1.492 O1 1.530 O4 1.543	- 0.987 1.001 0.985	1.02	1.15	0.26
		$B(OH)_4^-,Na^+$	O2 1.457 O1 1.455 O3 1.501 O4 1.514	0.990 1.005 0.992 0.989	0.88	0.38	0.58

719

720

721

722

723   Table 2: Experimental ^{11}B NMR parameters of synthetic and natural calcium carbonates

B coordinence		sample	δ_{iso} (ppm)	C_Q (MHz)	η	ref.[*]	present interpretation
trigonal	synthetic	calcite	17.1 ±1	3.0 ±0.3	0.67 ±0.05	1	$BO_2(OH)^{2-}$
		heated aragonite	22.0 ±1	2.7 ±0.3	0.2 ±0.05	1	BO_3^{3-}
		calcite	16.6 ±0.5	n.d.	n.d.	2	$BO_2(OH)^{2-}$
		Mg-calcite	16.5 ±0.5	n.d.	n.d.	2	"
		aragonite	18.9 ±0.5	2.8 ±0.1	n.d.	2	"
	natural	biogenic calcite	18.9 ±1	2.8 ±0.3	0.5 ±0.05	1	$BO_2(OH)^{2-}$
			19.3	2.6	0	3	BO_3^{3-}
		biogenic aragonite	16.8	2.5	0	3	$B(OH)_3$
			18.3	2.5	0	3	"
		coral CoC	17.5	2.3	0.2	4	"
tetragonal	synthetic	calcite	0.5 ±1	0.0 ±0.3	-	1	$B(OH)_4^-$
			1.9 ±0.5	n.d.	-	2	"
		calcite ("interstitial")	-0.3 ±0.5				?
		calcite ("interstitial")	-2.4 ±0.5				?
		Mg-calcite	1.2 ±0.5	n.d.	-	2	$B(OH)_4^-$
		aragonite	1.6 ±0.5	0.0 ±0.3	-	1	"
			1.6 ±0.5	n.d.	-	2	"
	natural	biogenic calcite	1.1 ±1	0.0 ±0.3	-	1	$B(OH)_4^-$
			1.67	0.0	-	3	"
		hydrothermal calcite	2.85	0.0		3	?
		biogenic aragonite	1.2 ±0.5	0.0 ±0.3	-	1	$B(OH)_4^-$
			2.54	0.0	-	3	?
			2.0	0.0	-	3	$B(OH)_4^-$
		coral CoC	1.5	0.1	-	4	"

724   [*]references: [1]Sen et al. (1994), [2]Mavromatis et al. (2015), [3]Klochko et al. (2009), [4]Rollion-Bard et al. (2011)

725

726

727 **Figure captions**

728

729 Figure 1: Theoretical structure of B-bearing calcite and aragonite obtained from first-

730 principles modeling. The H-bond with an oxygen atom of a neighboring carbonate group

731 is indicated by a dotted line. The star in the tetragonal models indicates the Ca atom

732 closest to boron, which has been selected to test the effect of Na^+ for Ca^{2+} substitution.

733 This atom is located at a distance of 3.09 Å and 3.05 Å from the boron atom in calcite and

734 aragonite, respectively.

735 Red: oxygen, blue: calcium, black: hydrogen, purple: carbon, green: boron.

736

737 Figure 2: Summary of first-principles metadynamic run on aragonite. The fluctuations of

738 SPRINT coordinates (top and middle panel) reflect the geometrical changes affecting the

739 H-bonding pattern of OH groups with O atoms belonging to surrounding carbonate

740 groups. The bottom panel reports the history dependent bias potential which drives the

741 system away from the previously explored configurations (see text). SPRINT

742 coordinates are defined through the product of the principal eigenvalue of the (real

743 valued) adjacency matrix with its corresponding eigenvector. To enforce invariance

744 under permutation of identical atoms, the resulting values are sorted in ascending order

745 within the oxygen and hydrogen subsets, and are shown with a color gradient ranging

746 from the lowest to the highest components.

747

748 Figure 3: Summary of first-principles metadynamic run on calcite. Legend as in Figure 2.

749

750

751   Figure 4: Theoretical and experimental ^{11}B NMR chemical shifts of trigonal boron. Full

752   symbols: theoretical values from Table 1, open symbols: experimental values from Table

753   2. The circles correspond to nil or weak η parameters; whereas the squares correspond

754   to high η values indicating in-plane distortion of the trigonal group. The triangles

755   correspond to experimental data for which the η parameter is lacking.

756

757   Figure 5: Theoretical and experimental ^{11}B NMR chemical shifts of tetragonal boron. Full

758   symbols: theoretical values from Table 1, open symbols: experimental values from Table
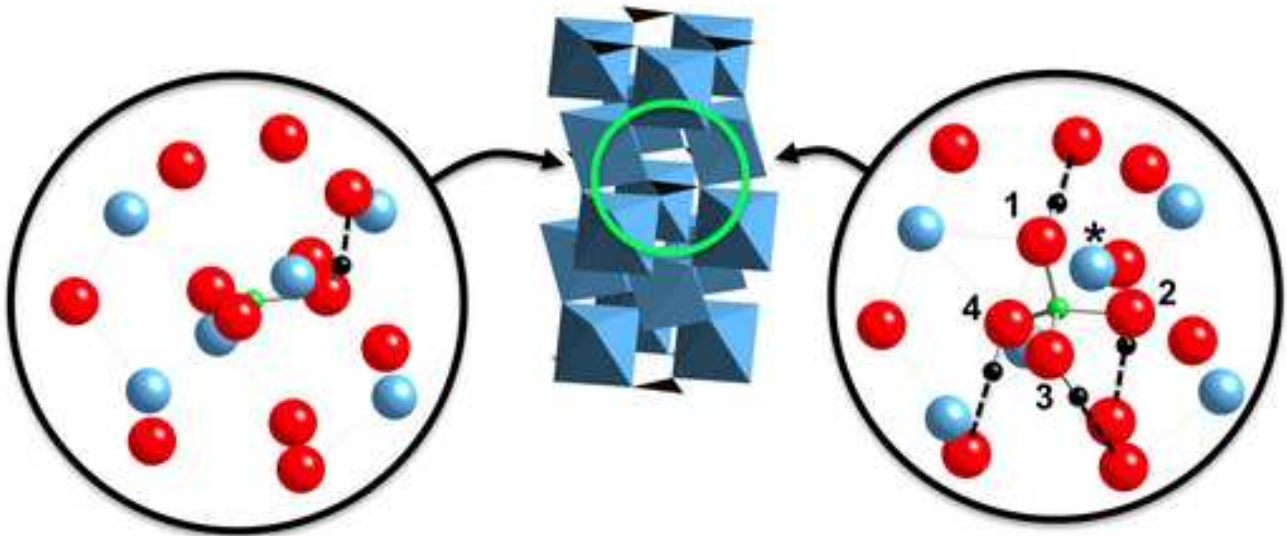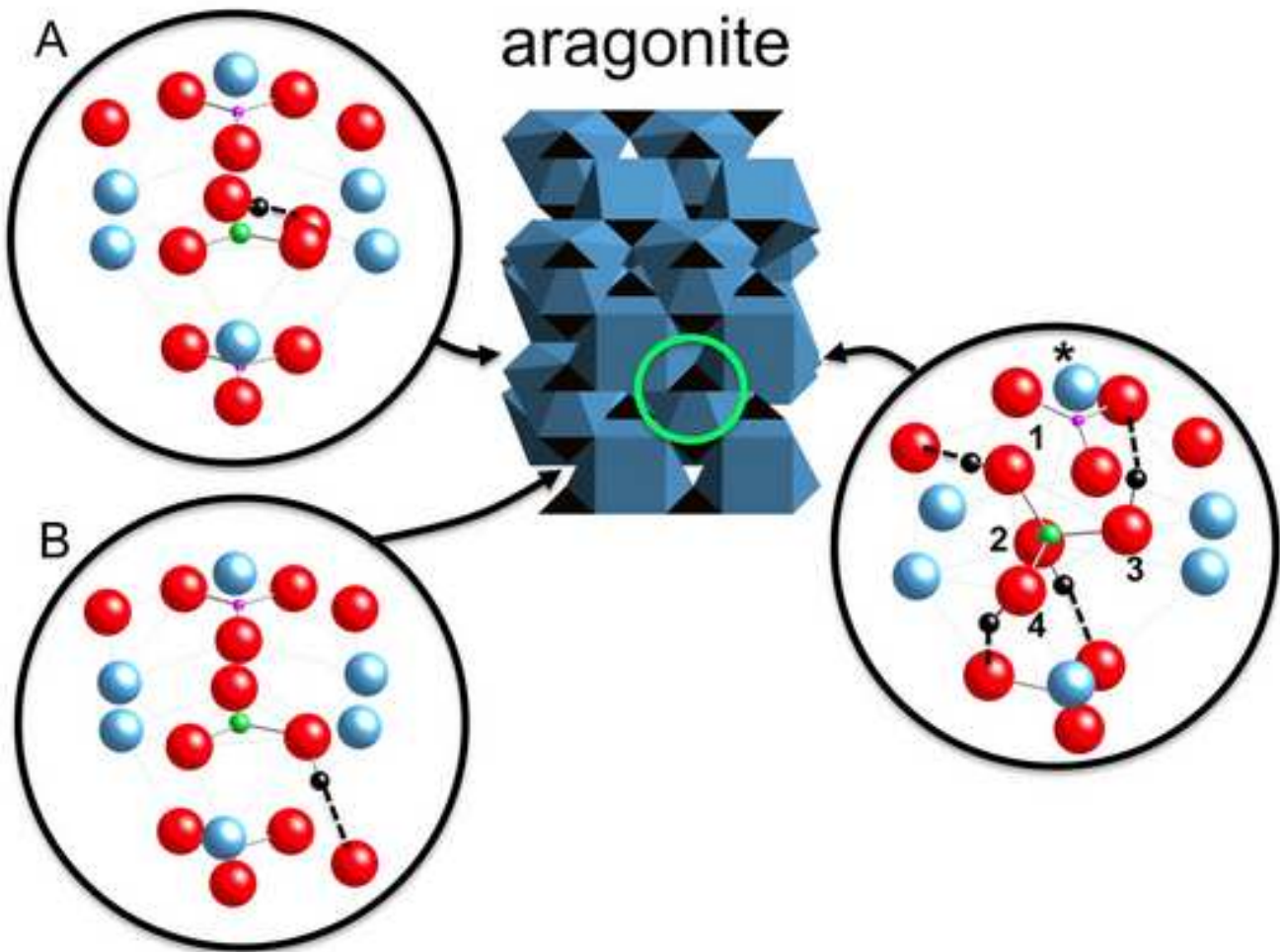
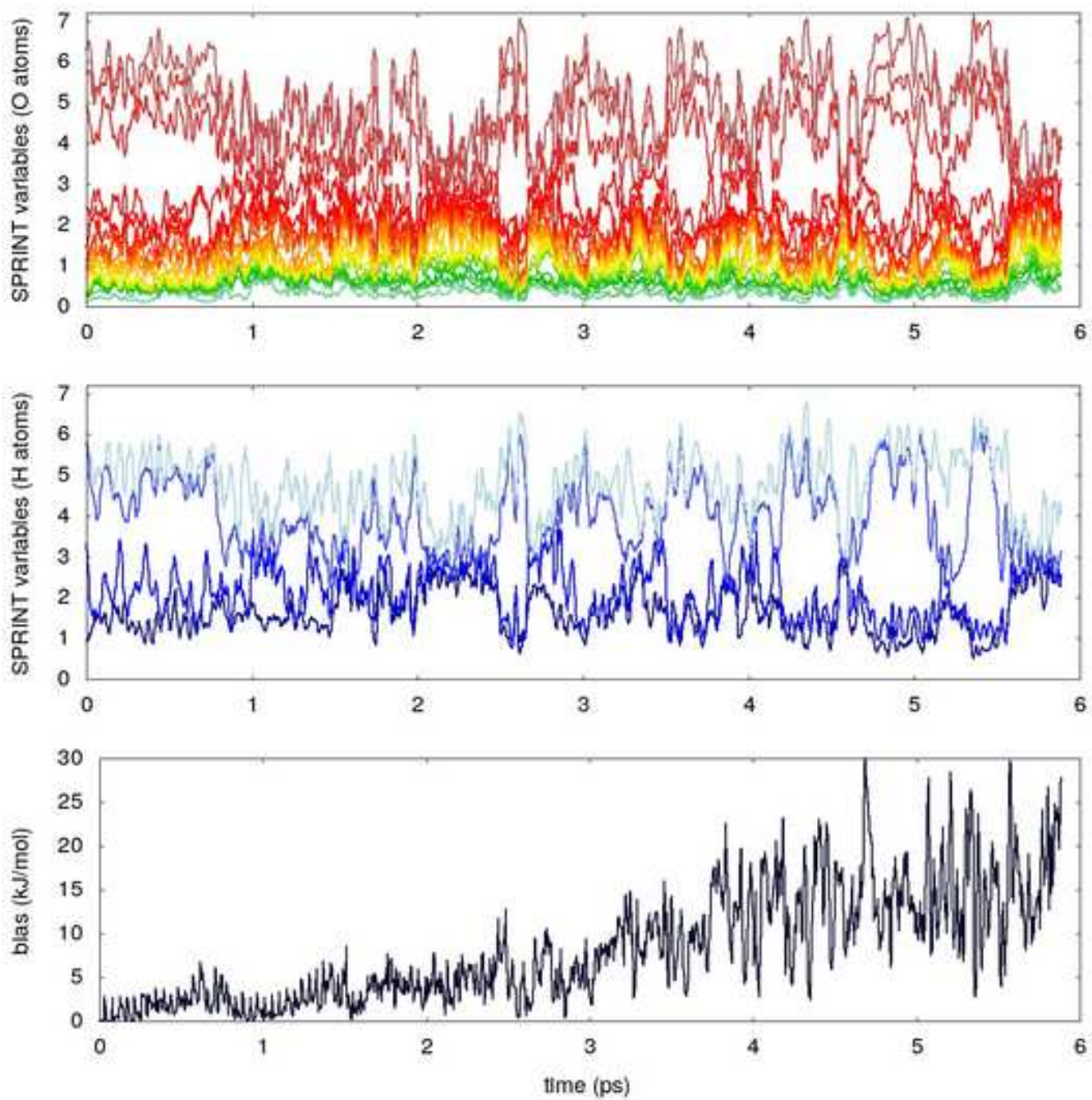759   2.

760

761

762

763

trigonal

tetragonal

calcite

aragonite

A

B

Summary of first-principles metadynamic run on aragonite.

Summary of first-principles metadynamic run on calcite.